Q. J. R. Meteorol. Soc. (2004), **130**, pp. 685–705 doi: 10.1256/qj.03.44

Adjoint sensitivity analysis of an observational operator for visible and infrared cloudy-sky radiance assimilation

By THOMAS J. GREENWALD*, TOMISLAVA VUKIĆEVIĆ, LOUIS D. GRASSO and
THOMAS H. VONDER HAAR
Cooperative Institute for Research in the Atmosphere, Colorado State University, Fort Collins, USA

(Received 12 March 2003; revised 29 September 2003)

SUMMARY

An adjoint modelling system is developed for an observational operator at visible and infrared wavelengths to explore the connection between cloud microphysics and top of atmosphere (TOA) radiances at cloud-resolving scales (2–5 km) in preparation for direct assimilation of cloudy-sky radiance satellite data. Analysis was performed on complex simulated three-dimensional cloud fields for different weather phenomena generated by the Regional Atmospheric Modeling System using two-moment microphysics. Sensitivity of TOA radiances at 0.63, 3.92, and 10.7 μm to changes in cloud mixing ratio revealed that small liquid drops and ice particles for very optically thin clouds were the largest contributors to the radiative sensitivities. More importantly, the sensitivities at these wavelengths were found to be complementary; i.e. 0.63 μm reflectances possessed greatest sensitivity to optically thinner water and ice clouds, whereas 3.92 μm responded to thick water clouds and to ice clouds, while 10.7 μm was most sensitive to thinner, cold ice clouds. Implications for numerical weather prediction (NWP) models that do not predict particle number concentration are that radiative sensitivities change somewhat in magnitude but retain the same sign, provided reasonable concentrations are assumed for broad classes of particle types. Overall, results indicated that satellite radiances measured in visible/infrared spectral windows contain potential information regarding cloud microphysics, especially at solar wavelengths, suggesting that direct assimilation of these data may be useful in supplying unique cloud information to NWP models.

KEYWORDS: Numerical weather prediction Radiative transfer modelling

1. INTRODUCTION

Direct assimilation of satellite radiance data into numerical weather prediction (NWP) models using variational techniques requires gradient information to adjust model initial conditions. These gradients, in part, come from the adjoint of an observational operator (OO) and are related to the partial derivatives of radiance at the top of atmosphere (TOA) with respect to three-dimensional (3D) NWP model control variables. Under clear-sky conditions these gradients are well known and understood (e.g. Eyre *et al.* 1993; Chevallier and Mahfouf 2001), and variational assimilation utilizing clear-sky radiance data has been conducted routinely and successfully over the past decade (Eyre *et al.* 1993; English *et al.* 2000). Under cloudy conditions, these gradients have been examined for radiative fluxes but limited to cloud fraction (Li and Navon 1998). To our knowledge, the characteristics of these gradients have not been investigated for visible and infrared radiances using cloud microphysical parameters. We believe a sensitivity analysis based on adjoint modelling and a direct physical link between radiances and microphysics, is an essential first step in understanding some of the potential these measurements may have in NWP, and in enabling their subsequent utilization by NWP models.

This study develops an adjoint system for a visible–infrared radiance OO (Greenwald *et al.* 2002) and, as a stand-alone system, examines its sensitivities to microphysical quantities under different modelled weather systems at traditional window wavelengths for space-based imagers (i.e. 0.63, 3.9, and 11 μm). The analysis is based on 1D radiative transfer (RT) theory and therefore has limitations, particularly at solar wavelengths. For horizontal grid spacing typical of climate models ($>\sim$60 km),

---

* Corresponding author, present address: SSEC/CIMSS, University of Wisconsin, 1225 W. Dayton Street, Madison, Wisconsin 53706, USA. e-mail: tomg@ssec.wisc.edu

subgrid-scale cloud optical-depth variability and cloud overlap have been found to be more important than 3D cloud effects, at least for broadband short-wave (SW) fluxes (Barker *et al.* 1998). This may also hold true for narrow-band SW radiances, although such studies have not been conducted. At cloud-resolving scales (less than a few km), however, effects of 3D cloud geometry on radiances and fluxes are likely to dominate over cloud overlap. Although studies are lacking that specifically address multidimensional effects on SW radiances at these spatial scales, their impact may be inferred from studies on the effects of cloud inhomogeneities on retrievals of cloud visible optical depth, which have been shown to be significant for oceanic stratocumulus (e.g. Chambers *et al.* 1997). It is, therefore, anticipated that 3D effects should also have an appreciable impact on radiative sensitivities at solar wavelengths; however, investigation of this topic is beyond the scope of this study.

Section 2 briefly describes the Regional Atmospheric and Modeling System (RAMS) used to generate 3D cloud fields. An overview of the OO is provided in section 3. Section 4 addresses the degree of linearity of the OO in order to provide insight into the suitability of the adjoint models in data assimilation. Section 5 describes the simulated 3D cloud fields used in the adjoint analyses. The RAMS, utilizing a sophisticated microphysics scheme, was used to produce hydrometeor vertical and horizontal structures that are as realistic as possible, and to resolve clouds at the spatial scale of the satellite measurements (2–5 km). Results of the adjoint analyses are discussed in section 6 followed by concluding remarks.

2. MESOSCALE MODEL DESCRIPTION

Simulations were conducted using RAMS version 4.29, which is a well-known and well-tested nonhydrostatic, cloud-resolving model (Pielke *et al.* 1992). Further technical aspects of RAMS can be found in Tripoli and Cotton (1982) and Tripoli (1986). Of greatest interest here are the RAMS microphysical parametrizations. Clouds and precipitation are explicitly predicted via a microphysics parametrization that features a one-moment scheme (mixing ratio) for cloud liquid water (Walko *et al.* 1995), and a two-moment scheme (mixing ratio and number concentration) for six other hydrometeor types, comprising: pristine ice, aggregates, snow, graupel, hail, and rain (Meyers *et al.* 1997). Snow and pristine ice are each further subdivided into different habits: columns, hexagons, dendrites, needles, and bullet rosettes, though none of these is predicted. Long-wave and SW radiative fluxes are parametrized using a two-stream model developed by Harrington (1997) that allows radiative heating to influence the growth of water droplets and ice particle vapour deposition (Harrington *et al.* 2000; Wu *et al.* 2000).

3. VISIBLE–INFRARED OBSERVATIONAL OPERATOR

The OO developed by Greenwald *et al.* (2002) is a system for practical computation of visible and infrared radiances in both clear and cloudy plane-parallel, multi-layer conditions. Cloud overlap is not considered, since it is less important at the relatively small spatial scales encountered in this study. The original system was applicable only to cloud droplets but is extended here to include other particle types. It features two different RT models, both of which handle multiple scattering: the Spherical Harmonic Discrete Ordinate Method (SHDOM, Evans 1998) at solar wavelengths, and a delta-Eddington two-stream approach (e.g. Deeter and Evans 1998) in the infrared. Special computational issues concerning SHDOM are discussed in appendix A. Gas extinction is computed based on the Optical Path TRANsmittance method (OPTRAN, McMillin *et al.* 1995). This system has been verified against GOES* imager data for forecasts of continental stratus (Greenwald *et al.* 2002).

Perhaps the most important component of the system is the conversion of microphysical information into particle single-scattering properties, i.e. extinction coefficient, single-scatter albedo and asymmetry factor. This is accomplished using anomalous diffraction theory (ADT, van de Hulst 1957), which allows for rapid calculation of these properties while maintaining a physical link to cloud microphysics. A modified form of ADT (Bryant and Latimer 1969), shown to be more accurate than the original theory introduced by van de Hulst (Sun and Fu 2001), is used here, based on the concept of an effective photon path (e.g. Mitchell 2002): $d_{\mathrm{e}} = V/P$, where V is particle volume and P is projected area. This distance is the quantity most relevant for describing the radiative properties of an individual particle or, when expressed as an effective particle diameter, a distribution of particles (Mitchell 2002). The key advantage of this approach is that any particle shape, no matter how complex, can be accommodated given its appropriate mass- and area-dimensional power law relationships (e.g. Mitchell 1996):

$$m = \alpha D^{\beta} \tag{1}$$

$$P = \gamma D^{\sigma} \tag{2}$$

where D is an effective diameter of the particle, m is mass, and α, β, γ, and σ are constants determined experimentally (see, e.g. Mitchell 1996). From these relationships, relatively simple and thus extremely computationally efficient, expressions may be obtained for the extinction coefficient and single-scatter albedo. The asymmetry factor, on the other hand, is computed somewhat differently based on traditional ADT (see Greenwald *et al.* 2002). In data assimilation, an ADT approach will allow for far easier exploitation of various kinds of satellite sensors and different particle types predicted by the forecast model than look-up table methods based on more rigorous calculations. ADT calculations have been verified against Lorenz–Mie theory (Mitchell 2000; Greenwald *et al.* 2002) and exact methods for hexagonal columns using T-Matrix methods (Mitchell, personal communication) with errors within 10%.

Cloud mixing ratio and number concentration for a collection of particles are brought into the ADT formulation in two ways. First it is assumed that the size distributions of different particle types may all be represented by the gamma distribution: $n(D) = N_0 D^{\nu} \mathrm{e}^{-\Lambda D}$, where ν is a width parameter in the gamma distribution, $\Lambda = (\nu + 1)/\bar{D}$, and $\bar{D}$ is the mean particle diameter. Both scattering and extinction efficiencies depend strongly on N_0, which is proportional to liquid-water content, and hence cloud mixing ratio (see Eq. (44) in Mitchell 2000). The second dependence comes through Λ since:

$$\bar{D} = (\nu + 1)\left(\frac{\Gamma(\nu + 1) r_{\mathrm{c}}}{\alpha \Gamma(\beta + \nu + 1) N_{\mathrm{c}}}\right)^{1/\beta} \tag{3}$$

where r_{c} and N_{c} are cloud mixing ratio and number concentration, respectively, and Γ denotes the gamma function; α, β, γ, and σ depend on particle type.

Table 1 shows values of α, β, γ, and σ assumed for the different particle types predicted by RAMS. Assigning these constants for the pristine ice and snow categories is difficult, given that they are composed of different habits which have different constants, and since the fraction of mass occupied by each habit is not known. For simplicity, pristine ice was assumed to be assemblages of polycrystals, similar to hexagonal plates

---

* Geostationary Operational Environmental Satellite.

TABLE 1. CONSTANTS ASSUMED FOR VARIOUS HYDROMETEOR TYPES IN THE POWER LAW RELATIONSHIPS[1]

Hydrometeor type	α	β	γ	σ
Cloud droplets	$\rho_w \pi/6$	3	$\pi/4$	2
Pristine ice	0.00739	2.45	0.2285	1.88
Aggregates	0.003	2.2	0.2285	1.88
Snow	0.003	2.2	0.2285	1.88
Graupel	0.049	2.8	0.5	2
Hail	0.466	3	0.625	2
Rain	$\rho_w \pi/6$	3	$\pi/4$	2

[1] Between mass and diameter (α and β) and projected area and diameter (γ and σ), where ρ_w is the density of liquid water.

(Mitchell 1996); snow was assumed to have the same constants as aggregates (Mitchell 1996). Also for simplicity, ν was fixed at a value of 6.0 for smaller hydrometeors (cloud drops and pristine ice) and 1.0 for larger particles (raindrops, hail, graupel, snow, aggregates). The tunnelling factor, which characterizes the degree that photons graze the particle edge and ranges between 0 and 1, was set to 1.0 for cloud drops and raindrops. This factor is less certain for irregularly shaped particles such as ice, and is a subject of current study (Mitchell *et al.* 2001); thus a value of 0.6 is assumed for all ice particle types. Also, Mitchell (2002) proposed the use of a bimodal size distribution in order to more accurately characterize cirrus scattering properties; however, for simplicity, a single mode distribution is employed here.

Of particular importance is how best to combine the scattering properties of a mixture of different hydrometeor types for input into the RT models. Mitchell and Arnott (1994) proposed weighting the extinction coefficients (β_{ext}) by the number concentration of each of the different ice particle types. Here, we obtain the total extinction due to hydrometeors as:

$$\beta_{\text{ext}} = \sum_{i=1}^{n} \beta_{\text{ext},i}, \tag{4}$$

where n is the number of hydrometeor types. The scattering parameters g and single scattering albedo ω_0 are weighted by projected area of the size distribution (Mitchell *et al.* 1996) as:

$$g_{\text{eff}} = \frac{1}{P_{\text{tot}}} \sum_{i=1}^{n} g_i P_i \tag{5}$$

$$\omega_{\text{eff}} = \frac{\beta_{\text{ext}}}{\beta_{\text{ext,tot}}} \frac{1}{P_{\text{tot}}} \sum_{i=1}^{n} \omega_{\text{o},i} P_i \tag{6}$$

where P_{tot} is the sum total of all projected areas, and $\beta_{\text{ext,tot}}$ is the total extinction due to hydrometeors and absorbing gases.

A simplification in the RT calculations not discussed by Greenwald *et al.* (2002) is that one calculation is made across the entire spectral width of the instrument channel. The instrument bandwidths are relatively narrow, so it is assumed that the Planck function and cloud scattering properties do not vary rapidly over these bandwidths. At infrared wavelengths, the errors are expected to be of the same order as errors in the two-stream model (~1.5 K). Errors may be somewhat larger near 3.7 μm due to rapid spectral changes in cloud scattering properties. Also, the use of the Henyey–Greenstein

TABLE 2. CHANNEL CHARACTERISTICS OF THE GOES-9 IMAGER AND ASSUMED REAL (N_r) AND IMAGINARY (N_i) PARTS OF COMPLEX REFRACTIVE INDICES FOR WATER AND ICE

		Water drops		Ice particles		
Channel	λ_m (μm)	n_r	n_i	n_r	n_i	Gas contributions
1	0.629	1.33	2.86×10^{-8}	1.31	1.72×10^{-8}	Atmospheric window, O_3 and weak water vapour
2	3.92	1.35	4.07×10^{-3}	1.37	0.00882	Atmospheric window
3	6.77	1.32	0.0362	1.32	0.0566	Upper tropospheric water vapour
4	10.72	1.17	0.0834	1.11	0.169	Atmospheric window, water vapour
5	12.01	1.13	0.204	1.28	0.408	Water vapour

The central wavelength λ_m is weighted by channel response function.

function to approximate the scattering phase function at visible wavelengths introduces additional errors (Greenwald *et al.* 2002). However, these various forward model errors may be incorporated into the observational error covariance matrix for data assimilation applications.

Table 2 lists the weighted mean wavelengths and refractive indices for water and ice used as input for the observational operator at each channel of the GOES-9 imager. As seen, channels 1, 2, and 4 potentially contain the most information about clouds due to less interference from atmospheric gases.

4. TESTS OF LINEARITY

The adjoint model is by definition an adjoint of the linearized forward nonlinear OO model (see appendix B for more discussion). This property of the adjoint model is exploited exactly in nonlinear variational data assimilation methods, in which a minimum of a so-called cost function is estimated by way of a gradient search in the space of control parameters through an iterative algorithm (e.g. Kalnay 2003). Limitations of this approach for strongly nonlinear OO models are that multiple cost-function minima, discontinuities, or the nonlinearities themselves may lead to a poor solution or even a divergence of the algorithm. It is, therefore, informative to determine the degree of linearity of the OO models to estimate the potential for this to occur.

The adjoint model solution also represents the linear sensitivity of the OO models to control parameters, and consequently is potentially useful for understanding physical dependencies between TOA radiances and properties of the atmosphere, clouds, and the surface. In the context of data assimilation, the sensitivity of the OO to control parameters is interpreted as information about the unobserved atmospheric and surface states contained in the observed radiances. Consequently, as long as the linear sensitivity is valid, the adjoint model solution can be used to study the potential information content of radiance observations. This is examined in section 6.

In this section the degree of linearity in the radiative response is investigated for cloud mixing ratio (CMR) perturbations. Although within a data assimilation environment perturbations in CMR could certainly exceed 100%, the upper limit chosen here is thought to be large enough to expose any significant nonlinearities in the OO. Two idealized cloud types were considered: an eight-layer low-level cloud (of depth 400 m in the boundary layer) composed of water droplets; and a two-layer cold cloud (of depth 2.4 km at ~12 km) consisting of pristine ice particles. In each case cloud mixing ratio is fixed throughout the cloud depth. Details concerning these calculations are given in Table 3.

TABLE 3. COMPUTED REFLECTANCES, BRIGHTNESS TEMPERATURES (T_b) AND CLOUD SCATTERING PROPERTIES AT THREE WAVELENGTHS FOR MODELLED OPTICALLY THICK AND THIN[1] LIQUID AND ICE CLOUDS USED IN THE LINEARITY EXPERIMENTS

	Liquid cloud			Ice cloud		
Wavelength (μm)	0.63	3.92	10.7	0.63	3.92	10.7
Reflectance or T_b (K)	0.785 (0.160)	295.3 (294.6)	286.3 (288.7)	0.840 (0.173)	282.8 (291.9)	213.7 (271.0)
Optical depth	80.1 (0.746)	90.6 (0.393)	89.2 (0.066)	71.1 (0.69)	73.6 (0.85)	69.2 (0.39)
Asymmetry factor	0.872 (0.788)	0.823 (0.701)	0.939 (0.264)	0.799 (0.715)	0.838 (0.818)	0.969 (0.827)
Single-scatter albedo	0.9999928 (0.9999994)	0.863 (0.975)	0.544 (0.144)	0.9999937 (0.9999985)	0.688 (0.895)	0.467 (0.243)

[1] Values for thin clouds are given in parentheses

Results for the liquid-water cloud are given for optically thin and thick clouds at upper (50 m from top) and lower (50 m from bottom) layers of the cloud, to contrast the responses for these different locations and extreme conditions (Fig. 1). At all wavelengths and in all conditions the responses are found to be highly linear (i.e. the perturbed OO results follow the tangent linear model results) except for the upper portions of the thick cloud at 0.63 μm. This behaviour is attributed to the nonlinear nature of RT in optically thick, highly multiple scattering media. In the lower portions of a very thick cloud, however, the response is instead linear, due to the significant reduction in photon scattering.

An extreme example of nonlinearity is shown for the upper layer of the thick ice cloud at 0.63 μm (Fig. 2). The degree of nonlinearity is greater than that for the low-level cloud because of negligible water vapour absorption in and above the cloud. Even though the absorption by boundary-layer water vapour for the low-level cloud is not exceptionally large, it is enough to reduce the probability of particle scattering and thus lessen nonlinearities.

A somewhat more unusual characteristic is seen in the upper layer of the thick ice cloud at 3.92 μm, a wavelength that includes both solar and thermal sources of radiation, where the response is strongly negative. Similar behaviour occurred for the low-level cloud at the topmost layer (results not shown). These negative responses are explained by a positive perturbation in CMR producing a negative perturbation in single-scatter albedo, implying greater absorption of solar radiation and thus a reduced brightness temperature.

The response at 10.7 μm for all optically thick clouds, no matter what the particle type and location within the cloud, is negligible due to the cloud behaving essentially as a black body. Negative responses for thin clouds are due to positive changes in extinction, since for larger CMR the cloud emits at a greater effective height, hence at colder temperature, with the effect generally being greatest at higher altitudes. Finally, indications of slight nonlinearities for all thin clouds at 3.92 μm and thin ice clouds at 10.7 μm are indirectly related to the nonlinear relationship between temperature and radiance (i.e. the Planck function), that is modified by changes in the weighting function as CMR is increased. These nonlinearities, however, are similar in magnitude to those encountered in clear sky for infrared wavelengths at or near strong molecular absorption lines (e.g. 6.7 μm).

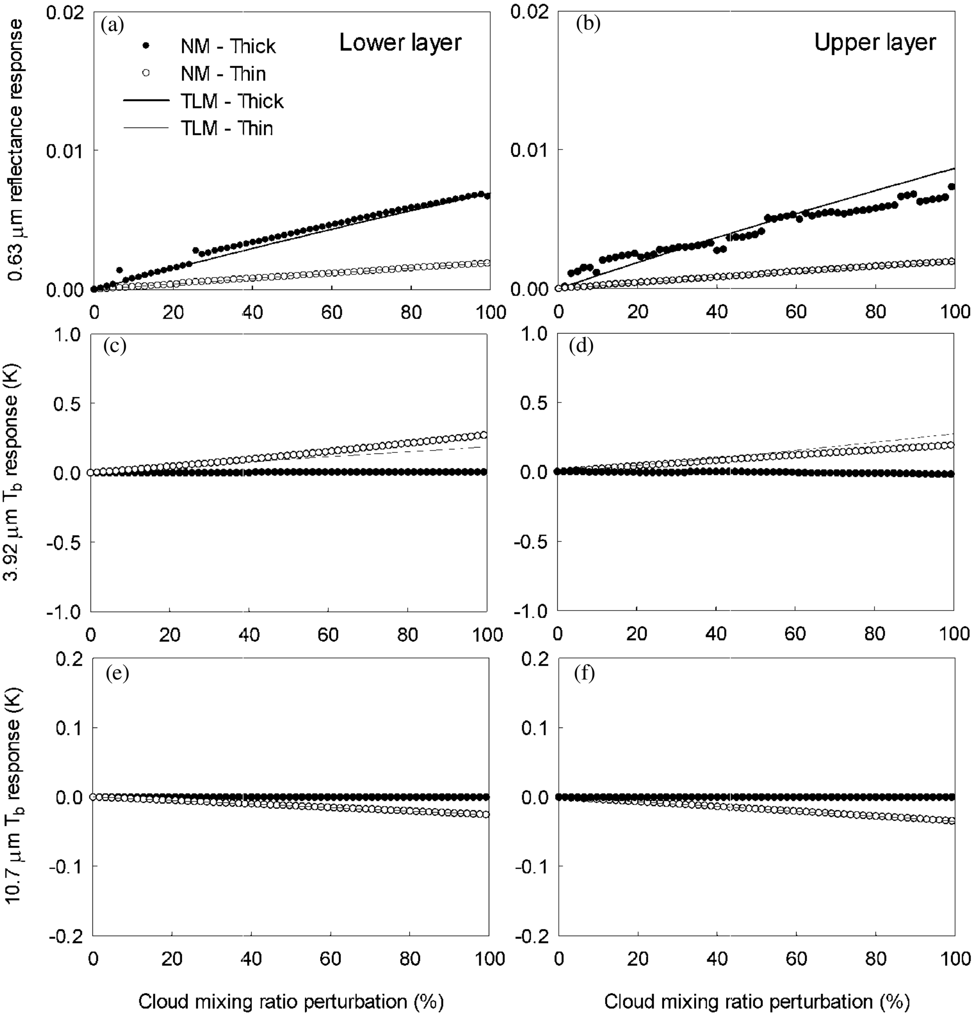

Figure 1. Reflectance responses at (a) 0.63 μm to relative mixing ratio perturbations at lower cloud layers for optically thin and thick low-level water clouds (see Table 3 for cloud optical depths). Calculations from both the nonlinear observational operator (OO) model (NM) and its tangent linear model (TLM) are shown. (b) As (a) but for upper cloud layers; (c) and (d) as (a) and (b) but for 3.92 μm brightness temperature (T_b); (e) and (f) as (a) and (b) but for 10.7 μm T_b. In all cases the following assumptions were made: a number concentration of 1.7×10^8 kg^{-1} ($\sim$287 cm^{-3}); a solar zenith angle of 30°; a relative solar azimuth of 100°; and a zenith angle of 45° for the upwelling radiance. The 'noisiness' of the perturbed nonlinear OO results for the thick cloud cases at 0.63 μm is due to the reduced accuracy of the Spherical Harmonic Discrete Ordinate Method (SHDOM, Evans 1998) solution in conditions of strong vertical gradients in extinction (see appendix A).

5. MESOSCALE MODEL SIMULATIONS

Three types of cloud systems were considered for examining sensitivities. The first case was the retrospective forecast of a warm stratus system over Oklahoma and Texas investigated by Greenwald *et al.* (2002). That study utilized a nested grid configuration (5 km fine spacing; 25 km coarse spacing; and 50 m vertical grid spacing in the boundary layer), with radiance calculations being performed on the fine grid. This study uses the same 5 km thermodynamical and microphysical fields. Figure 3 shows the spatial distribution of vertically integrated liquid-water field 15 hours into the forecast.

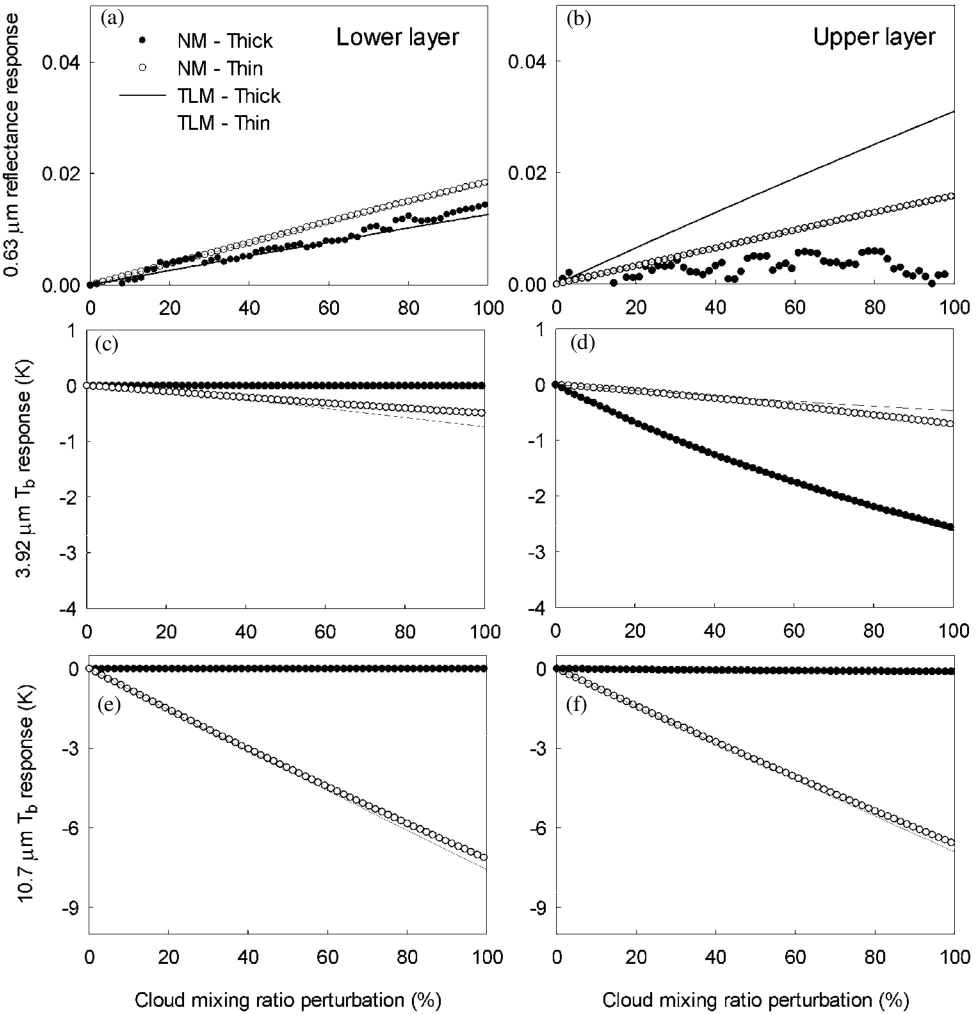

Figure 2. Same as Fig. 1 except for high-level ice clouds with a number concentration of 10^7 kg^{-1} ($\sim$17 cm^{-3}).

The second retrospective forecast was of a winter storm in the central USA on 2 March 2002. Three two-way interactive grids were utilized. The coarsest grid (horizontal grid spacing of 125 km) covered the western two thirds of the USA, while the next two grids (25 km and 5 km) included most of Kansas, Oklahoma, Missouri, and northern Arkansas. Vertical grid spacing was set as 500 m with a model top height of 20 km. All grids utilized two-moment microphysics and were initialized with 80 km Eta analysis data (originally derived from 12 km operational Eta Data Assimilation System analyses) at 00 UTC 2 March 2002. The total integrated water content field at 6 h into the forecast is shown in Fig. 4.

The final simulation was an idealized severe thunderstorm. The grid spacing was 4 km for the coarse grid, and 2 km for the fine grid in order to resolve the strong, localized updraught in the storm. The domain size was 400 by 400 km. Vertical grid spacing was 100 m in the lower atmosphere and gradually increased to 2 km at the top height of about 24 km. The atmospheric environment over the entire domain was

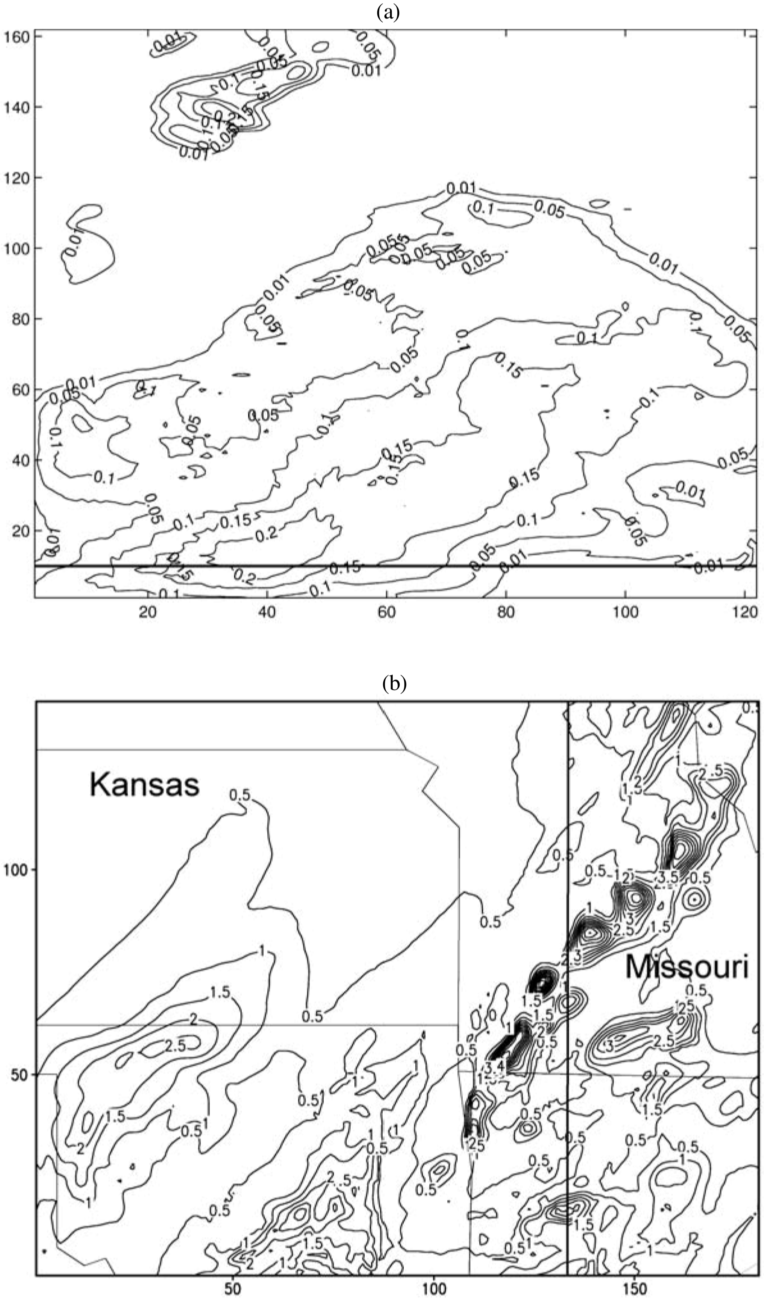

Figure 3. Vertically integrated total water content fields (kg m^{-2}) for: (a) the stratus and (b) the winter storm simulations. Bold horizontal and vertical lines show locations of the vertical cross-sections used in the adjoint analyses.

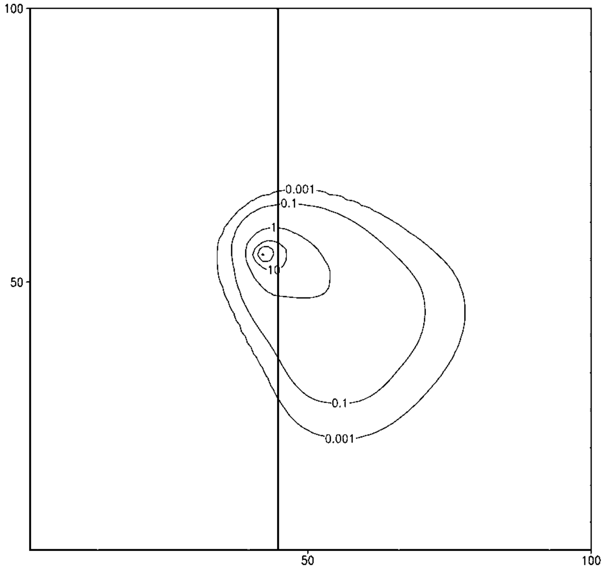

Figure 4. Same as Fig. 3 but for the thunderstorm simulation.

initialized with profiles of water vapour and temperature retrieved by the GOES-11 sounder at 2146 UTC 24 July 2000 in south-central Nebraska. Data for initializing the wind field were obtained from nearby wind-profiler sites at Neligh and McCook, Nebraska. The storm was initiated with a warm bubble and run for 2 h. At 115 minutes into the simulation (Fig. 4) the integrated water contents generally exceeded those of the stratus system, and in the updraught region those of the winter storm as well.

6. ADJOINT RESULTS

Of greatest interest in the sensitivity analysis is the contribution of changes in the mixing ratio (r) on the TOA radiances by all hydrometeor types. Solutions from the RT adjoint models and the ADT adjoint models were thus combined to provide the influence of all hydrometeors on the cost function (J) as:

$$\frac{\partial J}{\partial r} = \frac{\partial J}{\partial \beta_{\text{ext,eff}}}\left(\sum_{i=1}^{n} \frac{\partial \beta_{\text{ext},i}}{\partial r_i}\right) + \frac{\partial J}{\partial \omega_{\text{eff}}}\left(\frac{\beta_{\text{ext}}}{\beta_{\text{ext,tot}} P_{\text{tot}}} \sum_{i=1}^{n} \frac{\partial \omega_{\text{o},i}}{\partial r_i} P_i\right) + \frac{\partial J}{\partial g_{\text{eff}}}\left(\frac{1}{P_{\text{tot}}} \sum_{i=1}^{n} \frac{\partial g_i}{\partial r_i} P_i\right). \tag{7}$$

The adjoint model forcing was set exactly to unity, so the cost function gradients reduce to the Jacobians we are seeking (refer to (B.3)), i.e. $\partial\alpha/\partial r$ at 0.63 μm where α is reflectance, and $\partial T_{\text{b}}/\partial r$ at infrared wavelengths. The terms on the right-hand side of (7) are the contributions from the extinction coefficient, single-scatter albedo, and asymmetry factor, respectively, while the two components of each term derive from the RT adjoint model and ADT adjoint models (in parentheses).

Jacobians are supplied at each vertical level, and are computed for selected areas of three cases described below given 3D fields of temperature, pressure, water vapour

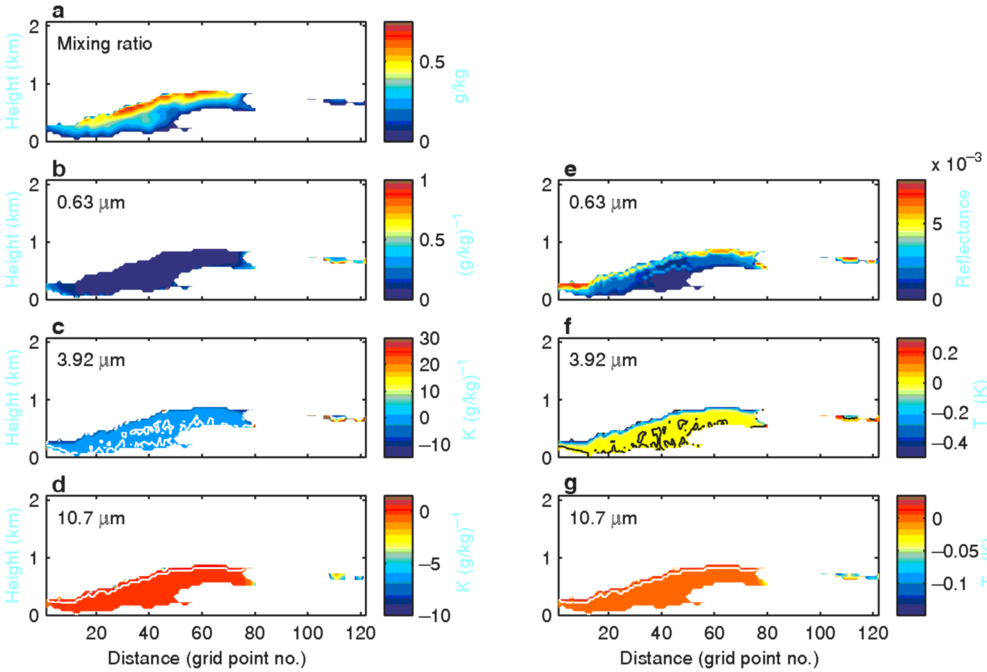

Figure 5. Vertical cross-sections for the stratus case along the line shown in Fig. 3(a) of: (a) the cloud mixing ratio field; (b), (c) and (d) the Jacobians at the three wavelengths shown; (e), (f) and (g) the scaled Jacobians at the same three wavelengths. Contours indicate division between positive and negative sensitivities.

mixing ratio, and hydrometeor mixing ratios/concentrations. Unless noted otherwise, all RT model input parameters (including surface properties) were set according to values in Table 5 of Greenwald *et al.* (2002). Solar zenith angle is assumed as 30° with a relative solar azimuth angle of 100°, while the zenith angle of the upwelling radiation is 45°. Cloud droplet number concentration was assumed in all cases as 1.7×10^8 kg^{-1}.

(*a*) *Stratus case*

Figure 5 shows results for a vertical cross-section through the southern part of the domain for the simulated stratus (see Fig. 3(a)). At all wavelengths the largest sensitivity occurs for the optically thinnest clouds (far-right portion of the domain and in certain localized areas) with very small sensitivities elsewhere. These results are somewhat misleading, however, since large gradients may occur that are not important relative to the base state of the cloud that is simulated. To account for this, ‘scaled’ results are also provided whereby the adjoint solution is multiplied by a perturbation. A similar type of scaling also occurs in the data assimilation process. Perturbations were assumed as a 15% change in mixing ratio for all hydrometeor types (in this case only cloud droplets) at each level.

Scaled Jacobian results for 0.63 μm show that the sensitivities extend deep within the cloud and are somewhat vertically correlated with cloud mixing ratio (cf. Fig. 5(a)). Optically thicker parts of the cloud system now have larger sensitivities. However, optically thinner clouds still generally have the largest sensitivities (e.g. far-left and right in Fig. 5(b)). This is mainly a result of the relationship between cloud reflectance and total optical depth, which is linear for optically thin clouds (hence greater sensitivity) but saturates for optically thick clouds (hence lower sensitivity). When separated into their

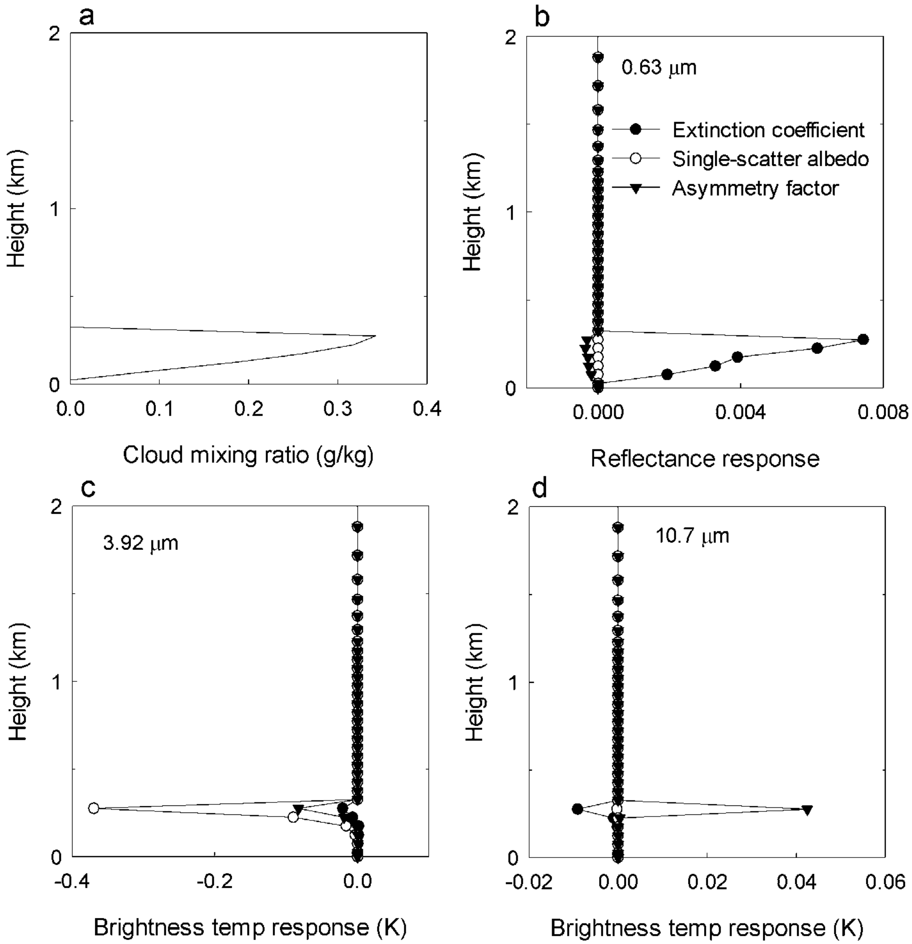

Figure 6. Vertical profiles at grid point #11 in Fig. 5 of: (a) cloud mixing ratio, (b) scaled sensitivities decomposed into contributions from cloud scattering parameters at 0.63 μm; (c) and (d) as (b) but at wavelengths of 3.92 and 10.7 μm, respectively.

three main components (i.e. extinction coefficient, single-scatter albedo, and asymmetry factor) the sensitivities for a moderately thick portion of the cloud are dominated by the extinction coefficient since extinction is strongly related to water content (see Fig. 6).

At 3.92 μm, which includes scattering of both solar and thermal radiation, the scaled sensitivity field is somewhat different from the Jacobian results, with the greatest sensitivities now negative and near the top of even the thickest clouds, except for extremely thin clouds where it can become positive (see Fig. 5). Again, the dominant term at this wavelength is the changes in the single-scatter albedo related to scattering of solar radiation (see Fig. 6). At 10.7 μm the scaled sensitivities are similar to the Jacobian results, with the optically thinnest clouds having by far the largest sensitivities.

(*b*) *Thunderstorm case*

In a cross-section through the simulated severe thunderstorm (Fig. 7), the Jacobian results at 0.63 μm indicate that the largest sensitivities occur in isolated areas of the uppermost part of the anvil, which can be either strongly negative or positive.

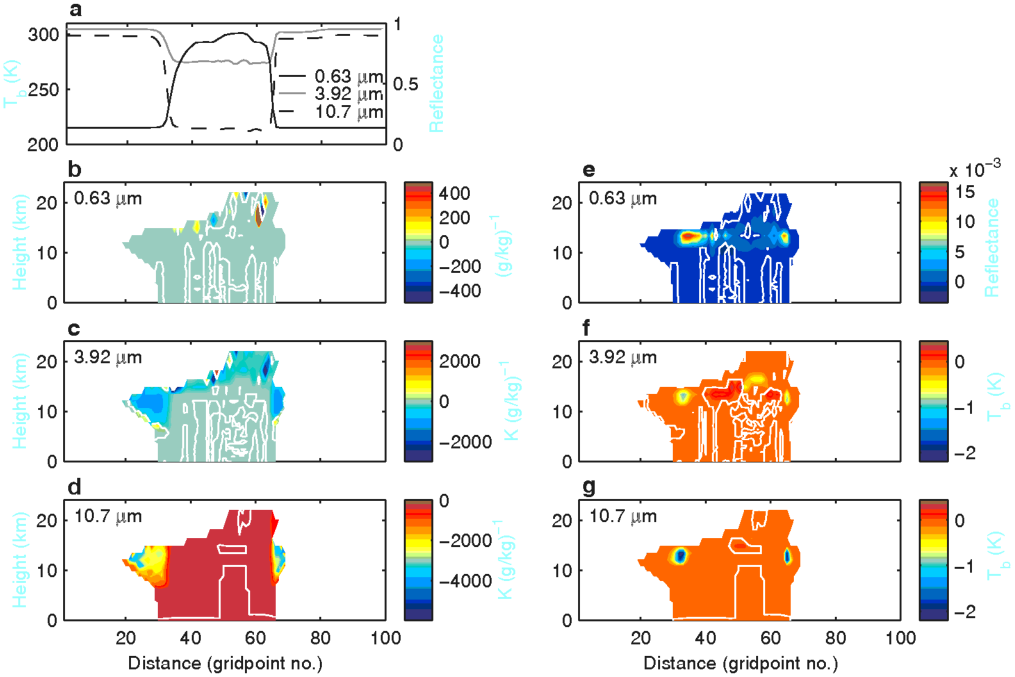

Figure 7. Same as Fig. 5 but for the thunderstorm case, except that here visible reflectances and infrared brightness temperatures (T_b) are shown in (a) in place of the cloud mixing ratio field.

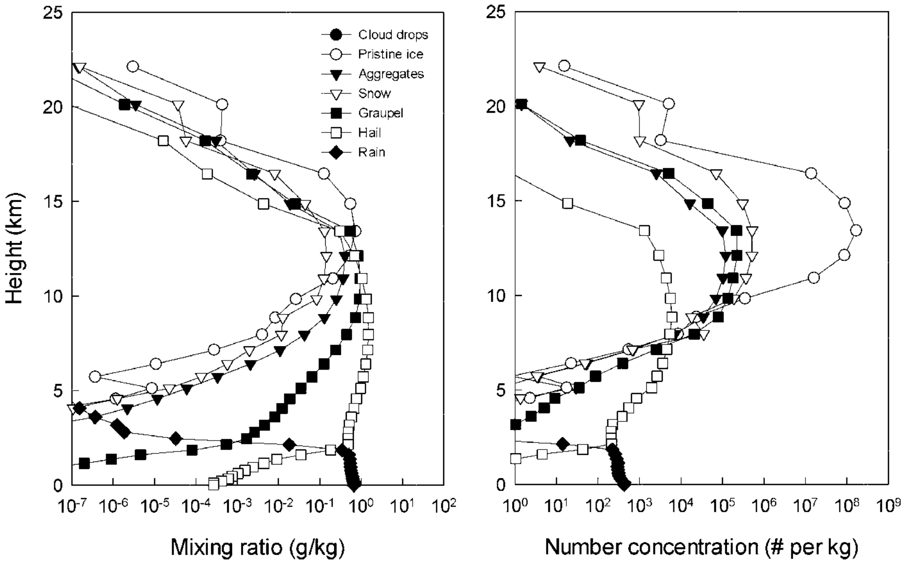

Figure 8. Vertical profiles for the thunderstorm simulation at grid point #57 in Fig. 7 of: hydrometeor mixing ratios (left), and number concentrations (right).

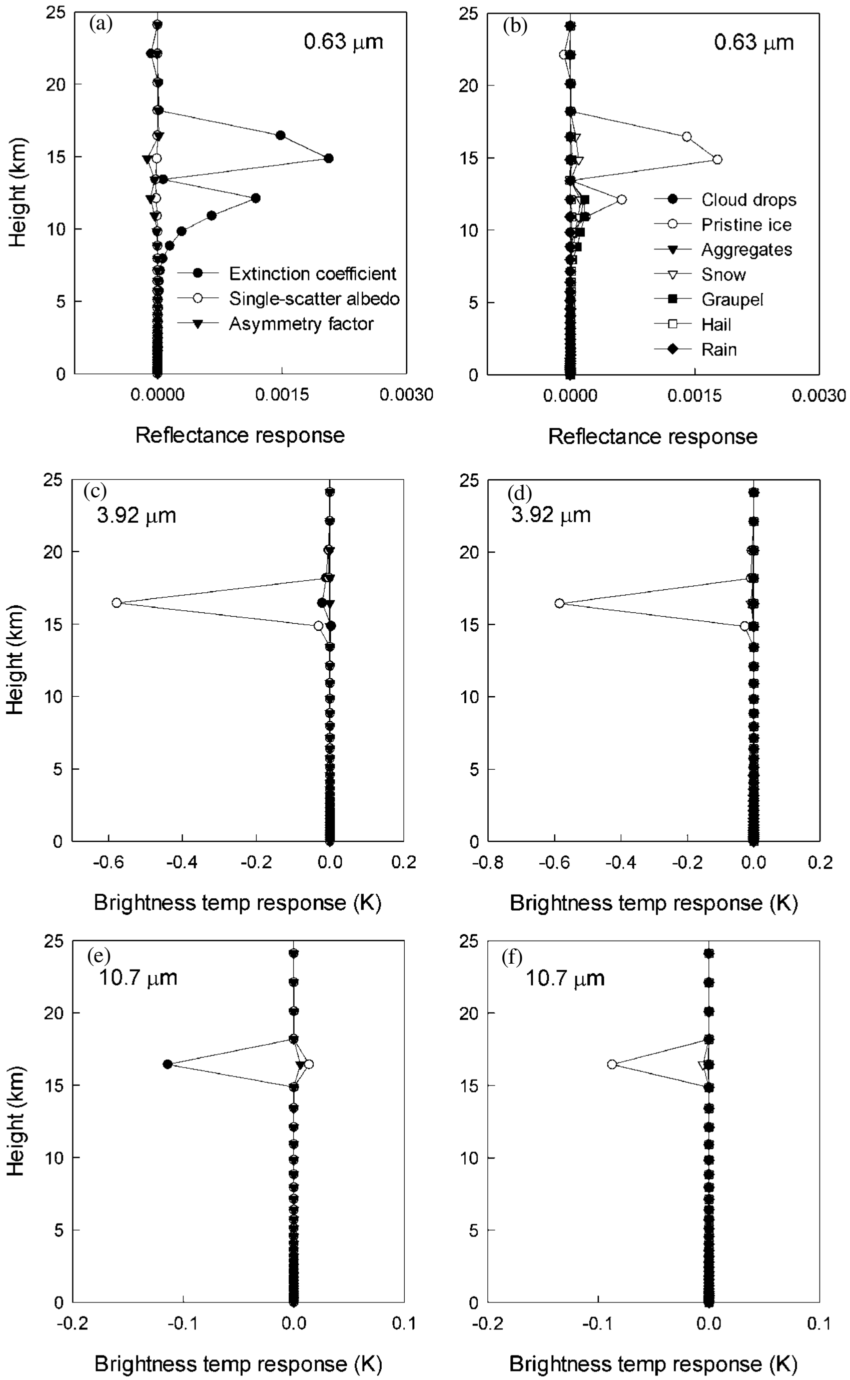

Figure 9. Vertical profiles of scaled sensitivities for the thunderstorm simulation at grid point #57 in Fig. 7 for: (a) reflectance response contributions from cloud scattering parameters at wavelength 0.63 μm; (b) as (a) but contributions according to hydrometeor type; (c) and (d) as (a) and (b) but brightness temperature response contributions at wavelength 3.92 μm; (e) and (f) as (c) and (d) but at wavelength 10.7 μm.

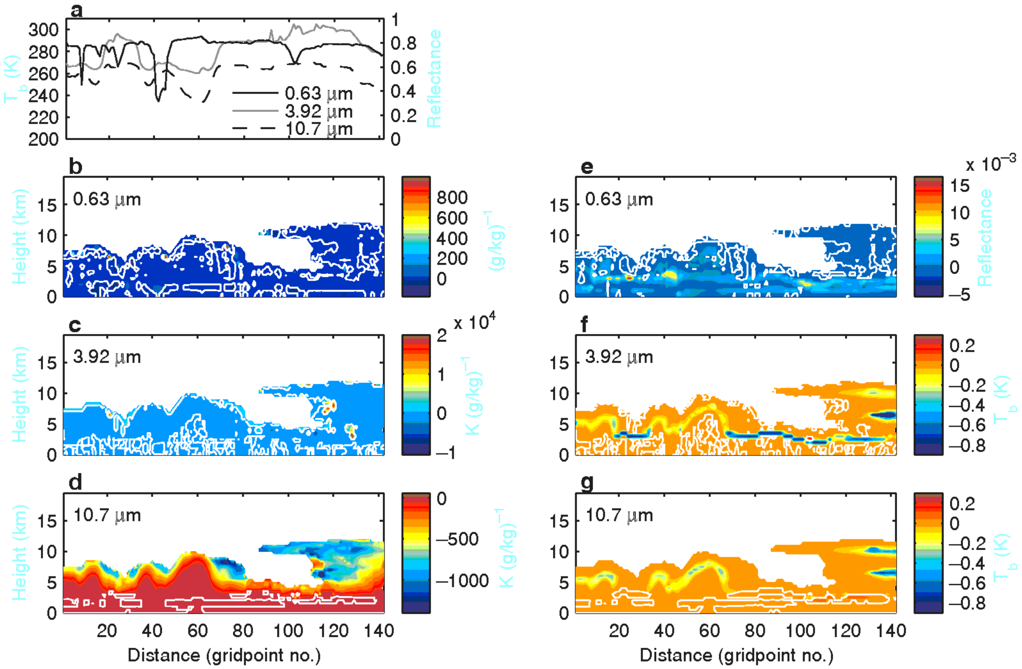

Figure 10. Same as Fig. 5 but for the winter storm case, except that here visible reflectances and infrared brightness temperatures (T_b) are shown in (a) in place of the cloud mixing ratio field.

Similar behaviour is seen at 3.92 μm, although very large negative sensitivities also exist at the optically thinnest parts of the cloud system, located near the fringes at 10 km. We should point out that these areas are extraordinarily thin, beyond detection by current satellite instrumentation. At 10.7 μm the dominant sensitivities are negative in these same regions, indicating that the sensitivities at 3.92 μm are the result of thermal emission.

The scaled results reveal a very different picture (Figs. 7(e)–(g)). Common to all wavelengths are the large sensitivities at the anvil ‘edges’ (i.e. from a radiometric point of view), which coincide with the largest horizontal gradients seen in the reflectance and brightness temperature fields. The response is particularly strong at 10.7 μm, reaching −2.2 K. Strong horizontal gradients in extinction due to rapid changes in pristine ice mixing ratios are mainly responsible for these high sensitivities.

Another area of interest is the core updraught region, where relatively high concentrations of large hail and graupel are found from mid-troposphere to the top of the boundary layer, and heavy rain within the boundary layer (Fig. 8). This region is exceptionally bright at 0.63 μm, approaching a reflectance of 0.9 owing to total optical depths exceeding 120. Significant variation in 3.92 μm brightness temperatures is also evident. Also associated with this region are very high concentrations of small ice particles at 10–17 km. Analysis of the scaled sensitivities in the updraught region (Fig. 9) indicates that pristine ice particles at these levels are the primary contributor, particularly at 3.92 μm. Although small, the 0.63 μm sensitivities even penetrate through the upper 7 km of the thunderstorm, unlike other wavelengths. Similar to the stratus case, the extinction coefficient and single-scatter albedo are also found to be the dominant terms at 0.63 μm and 3.92 μm, respectively. At 10.7 μm these sensitivities are negligible.

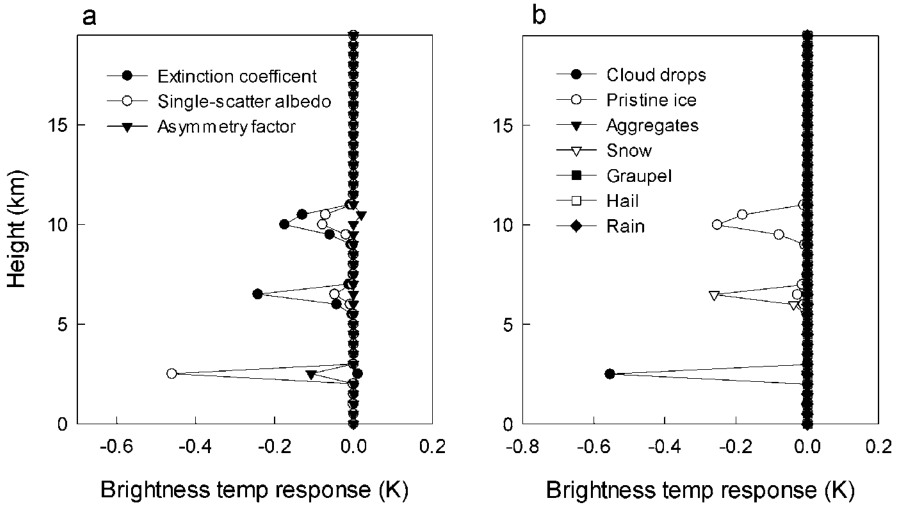

Figure 11. Vertical profiles of scaled sensitivities at 3.92 μm for the winter storm case at grid point #133 in Fig. 9, separated into contributions from: (a) cloud scattering parameters and (b) according to hydrometeor type.

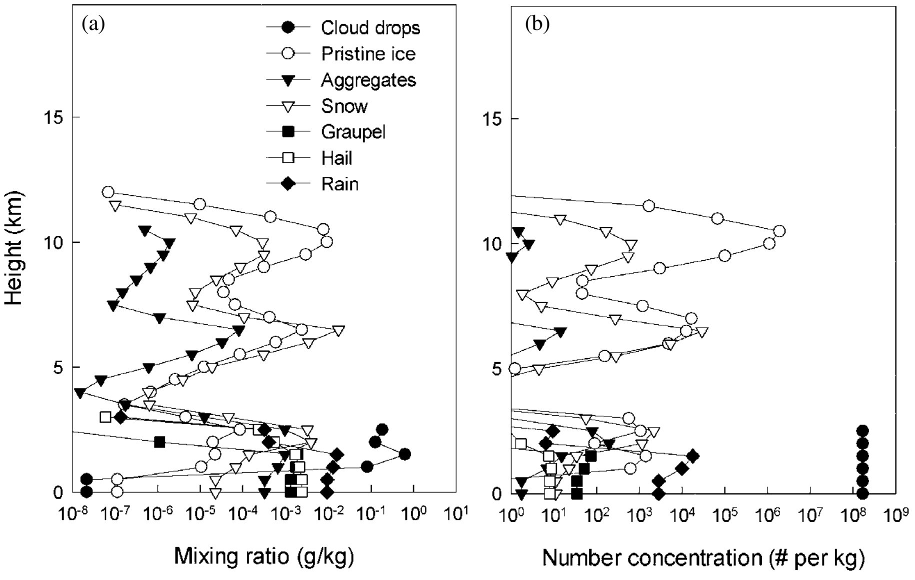

Figure 12. Vertical profiles for the winter storm at grid point #133 in Fig. 9 according to hydrometeor type of: (a) hydrometeor mixing ratios, and (b) number concentrations.

(*c*) *Winter storm case*

A wider variety of behaviour in the sensitivity fields was seen in the winter storm simulation because of more diverse cloud conditions. This diversity is reflected in the visible reflectance and brightness temperature fields for a north–south cross-section (see Fig. 3(b) for location) through western Missouri (Fig. 10(a)). This storm system was not nearly as deep as the thunderstorm simulation, and thus produced warmer 10.7 μm brightness temperatures. The largest values of the Jacobian at the solar wavelengths

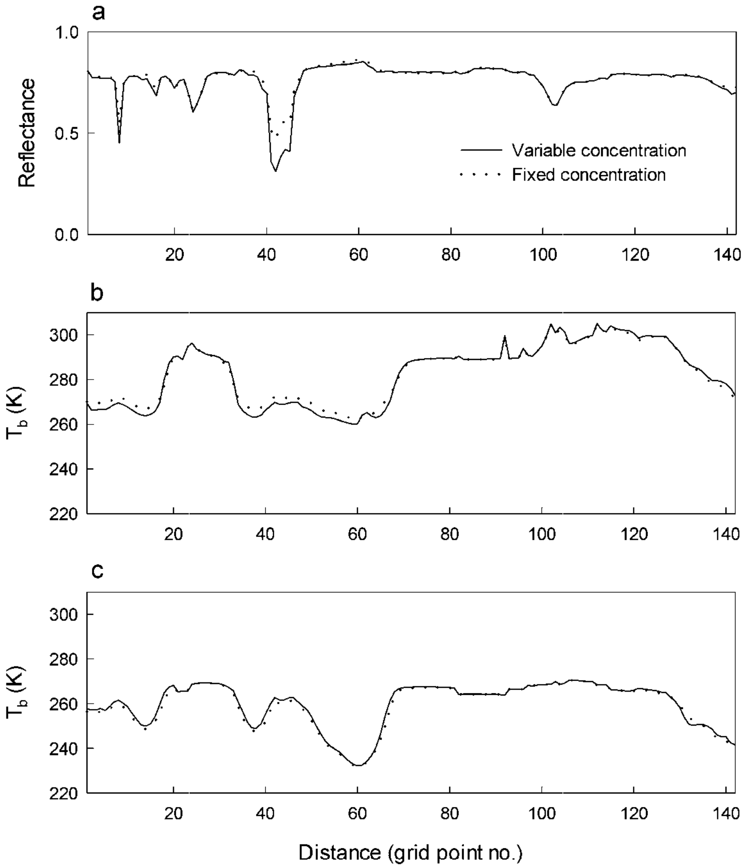

Figure 13. Calculations for the winter storm cross-section (see text) assuming predicted (variable) and fixed hydrometeor number concentrations of: (a) 0.63 μm reflectance; and (b) and (c) brightness temperatures (T_b) at 3.92 μm and 10.7 μm, respectively.

occurred in specific locations in the thinnest portions of the mid-altitude ice clouds and occasionally in water clouds at lower levels. At 10.7 μm the sensitivities were predominantly negative, with the largest appearing throughout the thinnest parts of the ice clouds.

Because the simulation produced a mainly thin ice canopy aloft and optically thick and extensive layers of cloud liquid water between 1 and 3 km, these liquid-water layers had a dominant radiative impact with respect to the scaled sensitivities at 0.63 μm and 3.92 μm. As seen in Fig. 10(e) the largest sensitivities at 0.63 μm generally coincided with relatively optically thinner clouds (i.e. those clouds with lower reflectances). When ice-cloud layers were not too optically thick (e.g. from grid points 20 to 30 and 70 to 142), 3.92 μm brightness temperatures had relatively high sensitivity to the upper optically thick liquid-water layers, unlike the 0.63 μm reflectances. In this respect, 3.92 μm brightness temperatures are highly complimentary to 0.63 μm reflectances in these situations. As expected, 10.7 μm brightness temperatures are generally insensitive to the liquid-water layers and respond mostly to microphysical changes in ice clouds, especially high and very thin clouds as seen in the far right portion of Fig. 10(g).

Perhaps the most noteworthy result is the sensitivity of the 3.92 μm brightness temperatures to multiple cloud layers (far right part of Fig. 10(f)). When examined in more detail, the extinction coefficient is found to contribute most of the sensitivity for the two upper cloud layers, and the single-scatter albedo at the lowest layer (Fig. 11). Sensitivities at the two upper cloud layers are mainly a consequence of thermal emission, whereas the sensitivity to the low-level cloud liquid-water layer comes about from the penetration of solar radiation through the optically thin (0.3–0.5) upper cloud layers. Interestingly, the response at the middle cloud layer is due principally to changes in snow mixing ratio, where high concentrations of large snow mixing ratios existed (Fig. 12).

Most, if not all, NWP models lack information concerning particle number concentration since this parameter is neither predicted nor diagnosed. This deficiency may have an impact on the forward computed radiances and the sensitivities. To investigate this further, calculations were performed again but this time smaller particles (i.e. pristine ice, aggregates, and snow) were assumed to have a fixed number concentration of 10^5 kg^{-1}, while large particles (i.e. graupel, hail, and rain) were assigned a lower concentration of 10^3 kg^{-1}. Results (not shown) indicate that the normalized sensitivities changed dramatically in only a few locations, but in all situations retained the same sign. Assuming fixed number concentrations appeared to have the largest effect on the radiances in certain cases (see Fig. 13). This was particularly evident at 3.92 μm where the differences were sometimes as large as 3–4 K, due to the greater sensitivity of radiances at this wavelength to microphysical characteristics. Large differences also occurred at 0.63 μm but only for the optically thinnest clouds.

7. CONCLUSIONS

An adjoint system was developed for an OO to examine the sensitivity of TOA radiances to cloud mixing ratio at selected visible and infrared wavelengths for various complex model-generated cloud fields. The major findings were:

- Response of the OO to cloud mixing ratio (assuming up to 100% perturbation) is linear to quasi-linear in all conditions, except in the upper levels of very optically thick ice clouds at visible wavelengths where strong nonlinearities exist.
- Small liquid drops and small ice particles contributed most to the sensitivities, with optically thin clouds generally producing the greatest sensitivities. Reflectances at 0.6 μm were most sensitive to optically thin and moderately thick clouds. At 3.92 μm, large negative scaled sensitivities were associated with thick water-cloud layers and in the thunderstorm anvil over the updraught region. Brightness temperatures at 10.7 μm were most sensitive to thinner, cold ice clouds. Radiances at these wavelengths thus provide a complimentary set of cloud microphysical sensitivities, with the solar wavelengths supplying the bulk of this information.
- Sensitivity of TOA radiances to cloud mixing ratio can occur deep within thick water clouds and thunderstorm anvils at 0.63 μm, and throughout optically thin clouds at 10.7 μm. Sensitivity to multiple cloud layers at 3.92 μm can also occur in certain cases.
- The inability to predict particle number concentrations in a NWP model appears to introduce only small to moderate uncertainties in the magnitude of the normalized sensitivities (the sign remains the same), provided a reasonable a priori estimate of the concentrations is given for broad classes of particle types. The largest impact, however, was on forward computed radiances, particularly at 3.92 μm, though significant errors were also seen at 0.63 μm for thin clouds.

One remaining challenge in fully utilizing the visible–IR OO and its adjoint in a 4D variational (4D-VAR) data assimilation system is specifying the background error covariance matrix for cloud mixing ratio (and number concentration if predicted). The nature of these error covariances is not well understood. In a recent 4D-VAR data assimilation study, assuming the error covariances for cloud mixing ratio are the same as for water vapour mixing ratio yielded good results (Vukićević *et al.*, personal communication); however, this assumption may not be appropriate in all situations. The next phase of our research is to better characterize these background-error statistics, and undertake further data assimilation experiments under a variety of cloudy weather phenomena in order to study in more detail the information content of satellite data in NWP under cloudy conditions.

ACKNOWLEDGEMENTS

This work was supported by the DOD Center for Geosciences/Atmospheric Research grant DAAL01-98-2-0078 and NOAA cooperative agreement NA7EC0676. Special thanks go to David Mitchell at the Desert Research Institute for supplying the ADT code and his helpful discussions. His work on modified ADT approaches was crucial in making the radiative transfer modelling system feasible. We also benefited from many stimulating discussions with our colleagues, Milija and Duska Zupanski and Andrew Jones. The comments of two anonymous referees are appreciated.

APPENDIX A

SHDOM computational considerations

Two important issues concerning SHDOM are the adaptive grid and the solution accuracy. In SHDOM the source function and radiance are defined on a discrete spatial grid. This grid is also adaptive, in the sense that it allows greater spatial resolution by further subdividing the cells of the fixed grid, to improve the solution accuracy. This process is referred to as 'cell splitting'. The criterion used for cell splitting depends on the local change of the source function in space, where splitting accuracy is scaled by the incoming solar flux. Extensive testing under a wide variety of cloud conditions has shown that the solution depends critically on the accuracy set for the adaptive grid cell splitting, especially when large vertical gradients in the cloud extinction, and subsequently the source function, occur. However, the use of high cell-splitting accuracy can significantly slow down radiance calculations. Since, here, accuracy is more important than speed, this study applies a single cell-splitting accuracy broadly across the entire spatial domain to achieve sufficient accuracy in all situations (Table A.1). Further investigation is needed, however, to determine the optimal cell-splitting accuracy for a given situation.

TABLE A.1. SCALE FACTORS FOR SOLAR FLUX USED TO DEFINE CELL-SPLITTING ACCURACY

Wavelength	Stratus	Thunderstorm	Winter storm
0.63 μm	0.003	0.03	0.01
3.92 μm	0.001	0.0001	0.001

Being an iterative method, SHDOM requires a threshold for the desired accuracy in the solution. Experience has shown that a value of at least 10^{-4} is needed to achieve sufficient accuracy in gradient calculations for the SHDOM tangent linear and adjoint models.

APPENDIX B

Adjoint model definitions

Let a nonlinear observational operator H act on a 2D vector of model state variables $\boldsymbol{x}$ (i.e. vertical profiles of mixing ratio, temperature, etc.) at a single grid point to produce a scalar monochromatic brightness temperature T_{b} as:

$$T_{\mathrm{b}} = H(x). \tag{B.1}$$

The response of T_{b} to all perturbations $\Delta x_1, \ldots \Delta x_N$, where N is the number of state variables, is obtained through a Taylor's series expansion of (B.1) retaining only the first order derivative term, called the tangent linear approximation:

$$\Delta T_{\mathrm{b}} = \sum_i \frac{\partial T_{\mathrm{b}}}{\partial x_i} \Delta x_i. \tag{B.2}$$

In the context of an optimization problem like data assimilation, we define a cost function J as some measure of the difference between the forward computed T_{b} and the observed T_{b}. The adjoint, defined here as the sensitivity of J to the input variables x_i, is thus derived by applying the chain rule to J (e.g. Errico 1997):

$$\frac{\partial J}{\partial x_i} = \sum_i \frac{\partial T_{\mathrm{b}}}{\partial x_i} \frac{\partial J}{\partial T_{\mathrm{b}}}, \tag{B.3}$$

where $\partial J/\partial T_{\mathrm{b}}$ is the so-called 'adjoint forcing' and $\partial T_{\mathrm{b}}/\partial x$ is often called the Jacobian. Although not obvious in (B.3), the key advantage of using an adjoint in sensitivity analysis is that the gradient need only be evaluated once for any arbitrary number of input variables, whereas traditional forward sensitivity analysis (e.g. applying the tangent linear) requires the forward model to be run separately for each input variable to produce a new perturbed value of the output.

REFERENCES

Barker, H. W., Morcrette, J.-J. and Alexander, G. D. 1998 Broadband solar fluxes and heating rates for atmospheres with 3D broken clouds. *Q. J. R. Meteorol. Soc.*, **124,** 1245–1271

Bryant, F. D. and Latimer, P. 1969 Optical efficiencies of large particles of arbitrary shape and orientation. *J. Colloid and Interface Sci.*, **30,** 291–304

Chambers, L. H., Wielicki, B. A. and Evans, K. F. 1997 Accuracy of the independent pixel approximation for satellite estimates of oceanic boundary layer cloud optical depth. *J. Geophys. Res.*, **102,** 1779–1794

Chevallier, F. and Mahfouf, J.-F. 2001 Evaluation of the Jacobians of infrared radiation models for variational data assimilation. *J. Appl. Meteorol.*, **40,** 1445–1461

Deeter, M. and Evans, K. F. 1998 A hybrid Eddington single-scattering radiative transfer model for computing radiances from thermally emitting atmospheres. *J. Quant. Spectrosc. Radiat. Transfer*, **60,** 635–648

English, S. J., Renshaw, R. J., Dibben, P. C., Smith, A. J., Rayer, P. J., Poulsen, C., Saunders, F. W. and Eyre, J. R. 2000 A comparison of the impact of TOVS and ATOVS satellite sounding data on the accuracy of numerical weather forecasts. *Q. J. R. Meteorol. Soc.*, **126,** 2911–2931

Errico, R. M. 1997 What is an adjoint model? *Bull. Am. Meteorol. Soc.*, **78,** 2577–2591

Evans, K. F. 1998 The spherical harmonics discrete ordinate method for three-dimensional atmospheric radiative transfer. *J. Atmos. Sci.*, **55,** 429–446

Eyre, J. R., Kelly, G. A., McNally, A. P., Andersson, E. and Persson, A. 1993 Assimilation of TOVS radiance information through one-dimensional variational analysis. *Q. J. R. Meteorol. Soc.*, **119,** 1427–1463

Greenwald, T. J., Hertenstein, R. and Vukićević, T. 2002 An all-weather observational operator for radiance data assimilation with mesoscale forecast models. *Mon. Weather Rev.*, **130,** 1882–1897

Harrington, J. Y. 1997 'The effects of radiative and microphysical processes on simulated warm and transition season Arctic stratus'. PhD thesis, Colorado State University

Harrington, J. Y., Feingold, G. and Cotton, W. R. 2000 Radiative impacts on the growth of a population of drops within simulated summertime Arctic stratus. *J. Atmos. Sci.*, **57,** 766–785

Kalnay, E. 2003 *Atmospheric modeling, data assimilation and predictability*. Cambridge University Press, Cambridge, UK

Li, Z. and Navon, I. M. 1998 Adjoint sensitivity of the earth's radiation budget in the NCEP medium-range forecasting model. *J. Geophys. Res.*, **103,** 3801–3814

McMillin, L. M., Crone, L. J., Goldberg, M. D. and Kleespies, T. J. 1995 Atmospheric transmittance of an absorbing gas, 4. OPTRAN: A computationally fast and accurate transmittance model for absorbing gases with fixed and variable mixing ratios at variable viewing angles. *Appl. Opt.*, **34,** 6269–6274

Meyers, M. P., Walko, R. L., Harrington, J. Y. and Cotton, W. R. 1997 New RAMS cloud microphysics parameterization. Part II: The two-moment scheme. *Atmos. Res.*, **45,** 3–39

Mitchell, D. L. 1996 Use of mass- and area-dimensional power laws for determining precipitation particle terminal velocities. *J. Atmos. Sci.*, **53,** 1710–1723

2000 Parameterization of the Mie extinction and absorption coefficients for water clouds. *J. Atmos. Sci.*, **57,** 1311–1326

2002 Effective diameter in radiation transfer: General definitions, applications and limitations. *J. Atmos. Sci.*, **59,** 2330–2346

Mitchell, D. L. and Arnott, W. P. 1994 A model predicting the evolution of ice particle size spectra and radiative properties of cirrus clouds. Part II: Dependence of absorption and extinction on ice crystal morphology. *J. Atmos. Sci.*, **51,** 817–832

Mitchell, D. L., Macke, A. and Liu, Y. 1996 Modeling cirrus clouds. Part II: Treatment of radiative properties. *J. Atmos. Sci.*, **53,** 2967–2988

Mitchell, D. L., Arnott, W. P., Schmitt, C., Baran, A. J., Havemann, S. and Fu, Q. 2001 Contributions of photon tunneling to extinction in laboratory grown hexagonal columns. *J. Quant. Spectrosc. Radiat. Transfer*, **70,** 761–776

Pielke, R. A., Cotton, W. R., Walko, R. L., Tremback, C. J., Lyons, W. A., Grasso, L. D., Nicholls, M. E., Moran, M. D., Wesley, D. A., Lee, T. J. and Copeland, J. H. 1992 A comprehensive modeling system—RAMS. *Meteorol. Atmos. Phys.*, **49,** 69–91

Sun, W. and Fu, Q. 2001 Anomalous diffraction theory for randomly oriented nonspherical particles: A comparison between original and simplified solutions. *J. Quant. Spectrosc. Radiat. Transfer*, **70,** 737–747

Tripoli, G. J. 1986 'A numerical investigation of an orogenic mesoscale convective system'. PhD thesis, Colorado State University

Tripoli, G. J. and Cotton, W. R. 1982 The Colorado State University three-dimensional cloud/mesoscale model—Part I: General theoretical framework and sensitivity experiments. *J. de Rech. Atmos.*, **16,** 185–219

van de Hulst, H. C. 1957 *Light scattering by small particles*. Dover Publications, New York, USA

Walko, R. L., Cotton, W. R., Meyers, M. P. and Harrington, J. Y. 1995 New RAMS cloud microphysics parameterization. Part I: the single moment scheme. *Atmos. Res.*, **38,** 29–62

Wu, T., Cotton, W. R. and Cheng, W. Y. Y. 2000 Radiative effects on the diffusional growth of ice particles in cirrus clouds. *J. Atmos. Sci.*, **57,** 2892–2904